Time-Domain vs. Frequency-Domain Equalization for FTN Signaling

Shuangyang Li *Student Member, IEEE*, Weijie Yuan *Member, IEEE*, Jinhong Yuan, *Fellow, IEEE,* Baoming Bai, *Senior Member, IEEE,* Derrick Wing Kwan Ng, *Senior Member, IEEE,* and Lajos Hanzo, *Fellow, IEEE*

***Abstract*—Faster-than-Nyquist (FTN) signaling has been recognized as a promising technique for next-generation high data rate communications. By intentionally reducing the symbol interval, FTN signaling is capable of transmitting more symbols than classic Nyquist signaling within the same time period and bandwidth. However, the intentional non-orthogonality of the bandlimited signaling pulses imposes severe inter-symbol interference (ISI), which requires powerful equalization at the receiver. Hence, we embark on the comparison of time- and frequency-domain equalization for FTN signaling both by theoretical analysis and numerical simulations. It is shown that frequency-domain equalization fails to reliably detect the FTN signal with a low FTN packing factor, while the time-domain equalization still performs well.**

***Index Terms*—FTN signaling, time-domain equalization, frequency-domain equalization.**

I. Introduction

Faster-than-Nyquist (FTN) signaling has attracted substantial attention since its discovery in 1970s [1]. In particular, FTN signaling is capable of increasing the spectral efficiency by transmitting data symbols faster than the Nyquist rate. In his pioneering paper [1], Mazo showed that when signaling transmits 25% faster than Nyquist rate, the minimum Euclidean distance between binary phase shift keying (BPSK) modulated sinc pulses remains the same, which indicates that FTN signaling can boost the data rate by 25% without performance degradation or bandwidth expansion. More importantly, it has been proved that FTN signaling can achieve a higher Shannon capacity than classic Nyquist signaling with a non-sinc signaling pulse [2], [3]. Therefore FTN signaling has been recognized as bandwidth-efficient signaling scheme, which has a great potential for supporting high speed data transmissions in next generation wireless communication systems [4], [5].

Recent advances of FTN signaling include the signal detection, code design, and related applications. For instance, in [6], a deep learning assisted FTN detector was presented, where a deep neural network (DNN) is concatenated to the factor graph of FTN signaling. By applying a revised message updating rule, this DNN-based detector is able to obtain superior error performance compared to that of conventional FTN detectors with almost the same detection complexity. Besides, a code based channel shortening scheme was presented in [7], where a special type of convolutional codes was applied to absorb the channel memory. Based on these convolutional codes, strong concatenated codes can be designed straightforwardly. Numerical results show that, incorporating with FTN signaling, the designed concatenated code not only reduces the detection complexity but also significantly enhances the error performance. More importantly, FTN signaling has been recently applied as an effective paradigm to enhance the spectral efficiency for various communication applications, such as multi-carrier transmission [8] and non-orthogonal multiple access (NOMA) [9].

Although FTN signaling has shown attractive features, it intentionally introduces intersymbol interference (ISI) at the transmitter side, which potentially imposes a high detection complexity. In particular, numerous reduced-complexity time-domain equalization (TDE) methods have been proposed, such as the M-algorithm-based Bahl-Cocke-Jelinek-Raviv (M-BCJR) algorithm of [10], [11]. However, the complexity of TDE increases exponentially with the ISI-duration. By contrast, frequency-domain equalization (FDE) relies on a single-tap multiplication, at the additional fixed complexity imposed by transforming the time-domain (TD) signal to the frequency-domain (FD) using the fast Fourier transform (FFT) [12]. More explicitly, given the circulant nature of the channel matrix, we can rely on single-tap sub-carrier equalization in the FD. To exploit the potential performance gain of FTN signaling, minimum mean square error (MMSE) based FDE was proposed in [13]. Furthermore, various variations of FDE have been proposed for FTN detection, such as the variational inference based method [14], [15], overlap FDE method [16]. In general, FDE relies on the Gaussian approximation of data symbols, which however inevitably results in performance loss. In a nutshell, both the TDE and the FDE have been widely applied for FTN detection. However, it has not been concluded in the open literature which one is more efficient at a given FTN packing factor τ.

This work was supported in part by the Australian Research Council Discovery Projects under Grant d DP190101363, in part by the Linkage Project under Grant LP170101196, in part by the National Natural Science Foundation of China under Grants 61771364, and in part by the Research and Development Project of Guangdong Province under Grant 2018B010114001. D. W. K. Ng is supported by funding from the UNSW Digital Grid Futures Institute, UNSW, Sydney, under a cross-disciplinary fund scheme and by the Australian Research Council's Discovery Project (DP190101363). L. Hanzo would like to acknowledge the financial support of the Engineering and Physical Sciences Research Council projects EP/N004558/1, EP/P034284/1, EP/P034284/1, EP/P003990/1 (COALESCE), of the Royal Society's Global Challenges Research Fund Grant as well as of the European Research Council's Advanced Fellow Grant QuantCom. (*Corresponding author: Weijie Yuan*).

S. Li is with the State Key Lab. of ISN, Xidian University, Xi'an 710071, China, and also with the School of Electrical Engineering and Telecommunications, University of New South Wales, Sydney, NSW 2052, Australia (e-mail: shuangyang.li@unsw.edu.au).

W. Yuan, J. Yuan, and D. W. K. Ng are with the School of Electrical Engineering and Telecommunications, the University of New South Wales, Australia (e-mail: weijie.yuan,j.yuan,w.k.ng@unsw.edu.au).

B. Bai is with the State Key Lab. of ISN, Xidian University, Xi'an 710071, China. (e-mail: bmbai@mail.xidian.edu.cn).

L. Hanzo is with the School of Electronics and Computer Science, University of Southampton, Southampton SO17 1BJ, U.K. (e-mail: lh@ecs.soton.ac.uk).

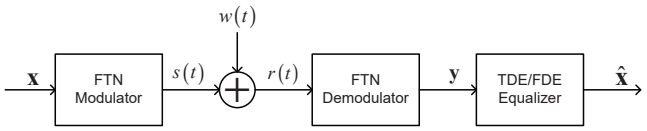

Fig. 1. System model of the FTN signaling system.

In this paper, we resolve this open dilemma for FTN transmissions over additive white Gaussian noise (AWGN) channels. Specifically, both the TD maximum-likelihood sequence estimation (MLSE) based on Ungerboeck observation model and the classic MMSE based single-tap FDE are investigated with special emphasis on their bit error rate (BER) upper bounds. We show that the detection complexity of the FDE is much lower than that of the TDE. However, the performance of the FDE is inferior to that of TDE due to: 1) the Gaussian approximation of the transmitted symbols; 2) the near-zero eigenvalues when τ is small. The simulation results verify the accuracy of our analysis and show that the TDE outperforms the FDE both in uncoded and coded systems, albeit at the cost of higher complexity.

Notations: Boldface capitals and lower-case letters are used to define a matrix and a vector, respectively; the superscripts $(\cdot)^{\mathrm{T}}$, $(\cdot)^*$, $(\cdot)^{\mathrm{H}}$ and $(\cdot)^{-1}$ denote the transpose, the conjugate, the Hermitian, and the inverse operations, respectively; $\mathrm{Re}(\cdot)$ denotes the real part of a complex number; $\Pr\{\cdot\}$ denotes the probability; $\mathbf{I}_N$ denotes an identity matrix of dimension N; $\mathbb{E}_x[\cdot]$, $\max_x[\cdot]$ and $\min_x[\cdot]$ denote the expectation, maximum and minimum operators with respect to the random variable x, respectively; $Q(\cdot)$ denotes the tail distribution of the standard normal distribution; $\propto$ represents both sides of the equation are multiplicatively connected to a constant; $\mathrm{tr}[\cdot]$ denotes the trace operator; notation $(\cdot)_{\mathrm{L}}$ denotes the lower triangular portion of a matrix without the main diagonal.

II. System Model

Without loss of generality, we consider a point-to-point FTN system model as shown in Fig. 1. Assume that a binary phase shift keying (BPSK) modulated symbol vector $\mathbf{x} = [x_0, x_1, ..., x_{N-1}]^{\mathrm{T}}$ of length N is transmitted with the FTN form of

$$s(t) = \sum_{n=0}^{N-1} x_n h\left(t - n\tau T\right), \tag{1}$$

where $h(t)$ is the T-orthogonal shaping pulse and τ is the FTN packing factor [1]. The received signal is $r\left(t\right) = s\left(t\right) + w\left(t\right)$, where $w(t)$ is the AWGN process with one-sided power spectral density (PSD) of N_0. After matched filtering and sampling at the FTN rate, the received symbol vector $\mathbf{y} = [y_0, y_1, ..., y_{N-1}]^{\mathrm{T}}$ is obtained as

$$\mathbf{y} = \mathbf{G}\mathbf{x} + \boldsymbol{\eta}, \tag{2}$$

where $\mathbf{G}$ is a Toeplitz matrix consisting of the ISI taps $g_i = \int_{-\infty}^{\infty} h\left(t\right) h^*\left(t - i\tau T\right) \mathrm{d}t$, such as

$$\mathbf{G} = \begin{pmatrix} g_0 & g_{-1} & \cdots & g_{1-N} \\ g_1 & g_0 & \cdots & g_{2-N} \\ \vdots & \vdots & \ddots & \vdots \\ g_{N-1} & g_{N-2} & \cdots & g_0 \end{pmatrix}. \tag{3}$$

In (2), $\boldsymbol{\eta}$ denotes the vector of colored noise samples with covariance matrix $\mathbb{E}_{\boldsymbol{\eta}}[\boldsymbol{\eta}\boldsymbol{\eta}^{\mathrm{H}}] = (N_0/2)\mathbf{G}$. In principle, FTN signaling can result in infinite ISI responses [17]. However, considering all ISI taps for equalization is impractical. As a compromise approach, the authors of [13], [17], consider a truncated version of $\mathbf{G}$ associated with the most recent L ISI taps, given by

$$\mathbf{H} = \begin{pmatrix} g_0 & g_{-1} & \cdots & g_{-L} & 0 & 0 & 0 & 0 & \cdots \\ g_1 & g_0 & g_{-1} & \cdots & g_{-L} & 0 & 0 & 0 & \cdots \\ \vdots & \ddots & \ddots & \ddots & & \ddots & & \ddots & \\ g_L & \cdots & g_1 & g_0 & g_{-1} & \cdots & g_{-L} & 0 & \cdots \\ 0 & g_L & \cdots & g_1 & g_0 & g_{-1} & \cdots & g_{-L} & \cdots \\ \vdots & & \ddots & & \ddots & \ddots & \ddots & & \ddots \end{pmatrix}. \tag{4}$$

On the other hand, FDE is performed by inserting a length-$2L$ cyclic prefix (CP) before applying the shaping filter and removing the CP (the first and last L samples) after the matched filter [13]. Specifically, we arrive at $\bar{\mathbf{H}}$, the circulant version of matrix $\mathbf{H}$ whose first row is given by $\{g_0, g_1, ..., g_L, 0, ..., 0, g_L, g_{L-1}, ..., g_1\}$.

III. Time-domain Equalization for FTN Signaling

The optimal TDE for uncoded FTN signals is based on the MLSE rule of

$$\hat{\mathbf{x}} = \arg\max_{\mathbf{x}} \Pr\left\{r\left(t\right)|\mathbf{x}\right\}. \tag{5}$$

For general ISI channels, two different observation models are commonly considered to perform MLSE, namely, the Forney observation model [18] and the Ungerboeck observation model [19], respectively. These two observation models are equivalent in terms of their detection performance. However, the Forney observation model can only handle the case where the noise samples are uncorrelated, i.e., white noise samples, while the Ungerboeck observation model is also applicable to colored noise samples. Notice that the FTN signaling has spectral zeros, when the symbol rate is higher than the signal bandwidth, i.e., $\tau < 1/(1+\beta)$ [20]. In this case, the Forney observation model cannot be directly derived [21]. Therefore, we consider the MLSE based on the Ungerboeck observation model to derive a general performance bound. Note that, Ungerboeck derived a performance bound for the Ungerboeck observation model of ISI channels in [19], where the corresponding ISI response is finite. However, when the channel has an infinite number of ISI components due to spectral zeros, the MLSE-based detector has to treat part of the ISI as additional noise. In other words, the detection is based on $\mathbf{H}$ instead of $\mathbf{G}$. According to [19], the metric of sequence $\mathbf{x}$ is defined as

$$J\left(\mathbf{x}\right) \triangleq \mathrm{Re}\left\{\mathbf{x}^{\mathrm{H}}\mathbf{y} - \frac{1}{2}g_0\|\mathbf{x}\|^2 - \mathbf{x}^{\mathrm{H}}\mathbf{H}_{\mathrm{L}}\mathbf{x}\right\}, \tag{6}$$

where

$$\mathbf{H}_{\mathrm{L}} \triangleq \begin{pmatrix} 0 & 0 & \cdots & 0 & 0 & \cdots \\ g_1 & 0 & 0 & \cdots & 0 & \ddots \\ g_2 & g_1 & 0 & 0 & \cdots & \ddots \\ \vdots & \ddots & \ddots & \ddots & \ddots & \ddots \\ 0 & g_L & \cdots & g_1 & 0 & 0 \\ \vdots & & \ddots & & \ddots & \ddots \end{pmatrix}. \tag{7}$$

Conventionally, (6) can be calculated by employing classic trellis-based algorithms having a complexity exponentially increasing with L. According to (6), the metric of the erroneous sequence (path) $\mathbf{x}+\mathbf{e}$ is then given by

$$\begin{aligned} &J(\mathbf{x}+\mathbf{e}) \\ =&\mathrm{Re}\left\{(\mathbf{x}+\mathbf{e})^{\mathrm{H}}\mathbf{y}-\frac{1}{2}g_0\|\mathbf{x}+\mathbf{e}\|^2-(\mathbf{x}+\mathbf{e})^{\mathrm{H}}\mathbf{H}_{\mathrm{L}}(\mathbf{x}+\mathbf{e})^{\mathrm{H}}\right\}. \end{aligned} \tag{8}$$

With respect to the trellis structure, a portion of an erroneous path that diverges/remerges from/to the correct path is termed as an error event $\mathcal{E}$ [22]. An error event will be declared, when the metric $J(\mathbf{x}+\mathbf{e})$ is higher than $J(\mathbf{x})$. To proceed, we define the normalized Euclidean distance as $d^2(\mathbf{e}) \triangleq \frac{1}{2E_b}\mathbf{e}^{\mathrm{H}}\mathbf{G}\mathbf{e}$ and the normalized *effective* Euclidean distance as $d^2_{\mathrm{eff}}(\mathbf{e}) \triangleq \frac{1}{2E_b}\mathbf{e}^{\mathrm{H}}\mathbf{H}\mathbf{e}$, respectively, where E_b is the average energy per information bit. Then we have,

$$\begin{aligned} &J(\mathbf{x}+\mathbf{e})-J(\mathbf{x}) \\ =&\mathrm{Re}\left\{\mathbf{e}^{\mathrm{H}}\mathbf{y}-g_0\mathbf{x}^{\mathrm{H}}\mathbf{e}-\frac{1}{2}g_0\|\mathbf{e}\|^2-2\mathbf{e}^{\mathrm{H}}\mathbf{H}_{\mathrm{L}}\mathbf{x}-\mathbf{e}^{\mathrm{H}}\mathbf{H}_{\mathrm{L}}\mathbf{e}\right\} \\ =&\mathrm{Re}\left\{\mathbf{e}^{\mathrm{H}}\mathbf{y}-\mathbf{e}^{\mathrm{H}}\mathbf{H}\mathbf{x}-E_b d^2_{\mathrm{eff}}(\mathbf{e})\right\}. \end{aligned} \tag{9}$$

Substituting (2) into (9) yields

$$J(\mathbf{x}+\mathbf{e})-J(\mathbf{x})=\mathrm{Re}\left\{\mathbf{e}^{\mathrm{H}}\boldsymbol{\eta}+\mathbf{e}^{\mathrm{H}}(\mathbf{G}-\mathbf{H})\mathbf{x}-E_b d^2_{\mathrm{eff}}(\mathbf{e})\right\}. \tag{10}$$

It can be observed in (10) that the term $\mathbf{e}^{\mathrm{H}}(\mathbf{G}-\mathbf{H})\mathbf{x}$ represents the influence of the residual ISI. Based on (10), the performance analysis can be carried out under the Gaussian assumption of $\mathbf{e}^{\mathrm{H}}(\mathbf{G}-\mathbf{H})\mathbf{x}$. Let us define the *equivalent* noise as $\varsigma \triangleq \mathrm{Re}\left\{\mathbf{e}^{\mathrm{H}}\boldsymbol{\eta}+\mathbf{e}^{\mathrm{H}}(\mathbf{G}-\mathbf{H})\mathbf{x}\right\}$ whose mean and variance are $\mathbb{E}[\varsigma]=0$ and $\mathbb{E}\left[\varsigma\varsigma^{\mathrm{H}}\right]=N_0E_bd^2(\mathbf{e})+2E_b\sigma^2_{\mathrm{ISI}}$, respectively, where $\sigma^2_{\mathrm{ISI}} \triangleq \frac{1}{2E_b}\mathbb{E}_{\mathbf{x}}[\mathbf{x}^{\mathrm{H}}(\mathbf{G}-\mathbf{H})\mathbf{e}\mathbf{e}^{\mathrm{H}}(\mathbf{G}-\mathbf{H})^{\mathrm{H}}\mathbf{x}]$ denotes the normalized variance of the residual ISI. Based on the Gaussian assumption, the occurrence probability $\Pr\{\mathcal{E}|\mathbf{e}\}$ of an error event is equivalent to the probability $\Pr\left\{\varsigma > E_b d^2_{\mathrm{eff}}(\mathbf{e})\right\}$. By invoking the Gaussian Q-function, $\Pr\{\mathcal{E}|\mathbf{e}\}$ is given by

$$\Pr\{\mathcal{E}|\mathbf{e}\} \lesssim Q\left(\sqrt{\frac{E_b}{N_0}d^2_{\mathrm{eff}}(\mathbf{e})\frac{d^2_{\mathrm{eff}}(\mathbf{e})}{d^2(\mathbf{e})+\frac{2\sigma^2_{\mathrm{ISI}}}{N_0}}}\right). \tag{11}$$

Based on (11), the BER bound can be derived by applying the union bound. Let us consider a set of error events $U(\mathcal{E}) \triangleq \left\{\mathcal{E}|N_{\mathcal{E}}=i, L_{\mathcal{E}}(i)=L_{\mathcal{E}}, w_{\mathcal{E}}=d^2_{\mathrm{eff}}(\mathbf{e})\right\}$, where $N_{\mathcal{E}}$ is the number of erroneous bits due to the error event $\mathcal{E}$, $L_{\mathcal{E}}(i)=L_{\mathcal{E}}$ is the error event length, and $w_{\mathcal{E}} = d^2_{\mathrm{eff}}(\mathbf{e})$ denotes the corresponding normalized *effective* Euclidean distance. Furthermore, let us denote the size of $U(\mathcal{E})$ as $N_U(\mathcal{E})$, and let $w_{\max}$ and $w_{\min}$ denote the maximum and minimum value of $w_{\mathcal{E}}$, respectively. We obtain the *cumulative information-weight enumerator* (CI-WE) of [22]–[24] as

$$B(W) \triangleq \sum_{i=1}^{N} B_{i,w_{\mathcal{E}}}W^{w_{\mathcal{E}}} = \sum_{i=1}^{N}\sum_{w_{\mathcal{E}}=w_{\min}}^{w_{\max}} \frac{N_U(\mathcal{E})}{2^{L_{\mathcal{E}}(i)-1}}W^{w_{\mathcal{E}}}, \tag{12}$$

where the term $1/2^{L_{\mathcal{E}}(i)-1}$ is the normalization factor assuming that each legitimate transmitted sequence $\mathbf{x}$ is produced with equal probability [25]. Thus, we can apply the simplified union bound to find the estimated BER based on (12). By assuming that only a single error event can happen for each FTN transmission, the BER can be estimated as [26]

$$P_b \lesssim \sum_{i=1}^{N}\frac{i}{N}B_{i,w_{\mathcal{E}}}Q\left(\sqrt{\frac{E_b}{N_0}w_{\mathcal{E}}\frac{w_{\mathcal{E}}}{d^2_{\mathcal{E}}(\mathbf{e})+\frac{2\sigma^2_{\mathrm{ISI}}}{N_0}}}\right), \tag{13}$$

where $d^2_{\mathcal{E}}(\mathbf{e})$ denotes the normalized Euclidean distance corresponding to the error event $\mathcal{E}$. It should be noted that (13) is not strictly an upper bound of the BER due to the simplifications of using the union bound and the Gaussian assumption of the residual ISI. An asymptotical approximation can be obtained by considering the expectation the residual ISI variance, i.e., by setting $\sigma^2_{\mathrm{ISI}} = \frac{1}{2E_b}\mathbb{E}_{\mathbf{x}}\left(\mathbf{x}^{\mathrm{H}}(\mathbf{G}-\mathbf{H})\mathbf{e}\mathbf{e}^{\mathrm{H}}(\mathbf{G}-\mathbf{H})^{\mathrm{H}}\mathbf{x}\right)$. It can be observed from (13) that the residual ISI will affect the exponential behaviour of the BER for TDE, leading to an error floor in the high-SNR region. If the value of σ^2_{ISI} is negligible, at the asymptotically high SNR, the BER for TDE will decay exponentially with the minimum effective Euclidean distance of error events. To calculate (13), we have to know the *effective* Euclidean distance corresponding to each error event. However, finding the distance spectrum is not straightforward and conventional methods cannot be directly applied for obtaining the distance spectrum due to the fact that the constellation mapping can be nonlinear. Therefore, we apply the method in [26] to find the spectrum, which is designed to compare all possible legitimate codewords using an efficient trellis search. Please refer to [26] for more details.

When the FTN signal is channel-coded, the optimal detection rule is the maximum *a posteriori* (MAP) rule. The MAP rule based on Ungerboeck observation model was firstly derived in the appendix of Ungerboeck's original paper [19]. However, a feasible implantation, i.e., BCJR algorithm based on the Ungerboeck observation model, was only introduced as late as in 2005 [27]. It should be noted that the *a priori* information gleaned from the channel decoder can be directly fed back to the TD equalizers relying on the BCJR algorithm, which is an important difference with respect to the FD equalizers of the following section.

IV. Frequency-domain Equalization for FTN Signaling

Mathematically, the eigenvalue decomposition of a circulant matrix is expressed as $\bar{\mathbf{H}} = \mathbf{F}^{\mathrm{H}}\boldsymbol{\Lambda}\mathbf{F}$, where $\mathbf{F}$ is the

discrete Fourier transform (DFT) matrix with the element on the ith row and kth column being $F_{i,j} = \frac{1}{\sqrt{N}} \exp(-\frac{j2\pi ik}{N})$ and $\mathbf{\Lambda} = \text{diag}\{\lambda_1, ..., \lambda_N\}$ is the matrix of sorted eigenvalues of $\bar{\mathbf{H}}$. To employ FDE, the received samples are transformed to the FD as

$$\begin{aligned}\mathbf{F}\mathbf{y} = \mathbf{y}_f &= \mathbf{F}\bar{\mathbf{H}}\mathbf{x} + \mathbf{F}\boldsymbol{\eta} = \mathbf{F}\mathbf{F}^{\mathrm{H}}\mathbf{\Lambda}\mathbf{F}\mathbf{x} + \boldsymbol{\eta}_f \\ &= \mathbf{\Lambda}\mathbf{x}_f + \boldsymbol{\eta}_f, \end{aligned} \tag{14}$$

where $\boldsymbol{\eta}_f$ has an autocorrelation function given by $N_0\bar{\mathbf{G}}$ and $\bar{\mathbf{G}} = \mathbf{F}\mathbf{G}\mathbf{F}^{\mathrm{H}}$.

Taking the identical symbol probabilities of $\mathbf{x}$ into consideration, we have the FD mean and covariance matrix for $\mathbf{x}_f$, given by $\mathbf{0}$ and $E_s\mathbf{I}_N$, respectively. Consequently, the MMSE estimator can be used as[1],

$$\hat{\mathbf{x}}_f = \arg\min_{\mathbf{x}_f} \|\hat{\mathbf{x}}_f - \mathbf{x}_f\|^2 = \mathbf{W}\mathbf{y}_f. \tag{15}$$

Following some straightforward manipulations, the weight matrix $\mathbf{W}$ is given by

$$\mathbf{W} = \mathbf{V}_{x_f}\mathbf{\Lambda}^{\mathrm{H}} \left(\mathbf{\Lambda}\mathbf{V}_{x_f}\mathbf{\Lambda}^{\mathrm{H}} + N_0\bar{\mathbf{G}}\right)^{-1}, \tag{16}$$

where $\mathbf{V}_{x_f} = E_s\mathbf{I}_N$. In general, the computational complexity of a matrix inverse operation is of a cubic order with respect to its dimension. To reduce the computational complexity, we approximate the matrix $\bar{\mathbf{G}}$ by a diagonal matrix $\mathbf{\Phi} = \text{diag}\{\Phi_1, ..., \Phi_N\}$ comprised of $\bar{\mathbf{G}}$'s main diagonal entries as proposed in [16], [28]. Consequently, $\mathbf{W}$ is constructed as a diagonal matrix and the MMSE estimator can be operated on a symbol-by-symbol basis, yielding $\hat{x}_{f,n} = W_{n,n}y_{f,n}$, where $\hat{x}_{f,n}$ is the nth element in $\hat{\mathbf{x}}_f$. By adopting this approximation, the FD symbols are transmitted independently on N sub-carriers (sub-channels) with the channel power gain for the nth sub-carrier $\{\lambda_n\}$. The equivalent SNR corresponding to the nth sub-carrier is $\lambda_n E_s/N_0$, where E_s is the average symbol energy. Due to the Gaussian approximation of the data symbols, equations (9)-(13) are not applicable to analyze the performance of FDE. Instead, we apply the BER upper bound derived by Adachi [29],

$$\text{BER} \leq Q\left(\sqrt{\gamma(E_s/N_0)}\right), \tag{17}$$

where $\gamma(E_s/N_0)$ is regarded as the equivalent SNR for BPSK modulation, given by

$$\gamma(E_s/N_0) = \frac{\frac{2E_s}{N_0}\left|\frac{\sum_{n=1}^{N}\hat{\lambda}_n}{N}\right|^2}{\frac{\sum_{n=1}^{N}|W_{n,n}|^2}{N} + \frac{2E_s}{N_0}\cdot\left(\frac{\sum_{n=1}^{N}|\hat{\lambda}_n|^2}{N} - \left|\frac{\sum_{n=1}^{N}\hat{\lambda}_n}{N}\right|^2\right)},$$

with $\hat{\lambda}_n = W_{n,n}\lambda_n$. This upper bound offers an accurate prediction for the actual BER of the FDE.

It should be noted that the eigenvalues of $\bar{\mathbf{H}}$ are of great importance for FDE. However, it can be shown that the eigenvalues of $\bar{\mathbf{H}}$ exhibit similar behaviour to that of $\mathbf{H}$ and $\mathbf{G}$, which are bandlimited, complying with the shape of the folded spectrum [20]. As $\mathbf{H}$ is a truncated version of $\mathbf{G}$, the eigenvalues of $\mathbf{H}$ and $\mathbf{G}$ are almost the same if the truncation length L is sufficiently high to collect most of the ISI energy. On the other hand, it has been shown in [30] that there is an asymptotic equivalence of the Toeplitz matrix and its corresponding circulant approximation, where the difference between their eigenvalues tends to zero as the matrix size tends to infinity. Hence, it is natural to expect that the eigenvalues of the Toeplitz matrix $\mathbf{H}$ and its circulant approximation $\bar{\mathbf{H}}$ are of similar values to that of $\mathbf{G}$. Note that this conclusion can be directly obtained by applying Theorem 2 in [30]. To verify this assumption, we also calculate the eigenvalues of $\mathbf{G}$, $\bar{\mathbf{H}}$, and $\mathbf{H}$ both for $\tau = 0.8$ as well as for $\tau = 0.35$ and plot them in the descending order in Fig. 2. Specifically, we consider the use of a root raised cosine (RRC) signaling pulse with a roll-off factor $\beta = 0.3$ and we truncate the corresponding matrix $\mathbf{G}$ by using $L = 8$ and $L = 20$ for $\tau = 0.8$ and $\tau = 0.35$, respectively, which are sufficiently large to collect the most of the ISI energy [10]. Here we observe that the eigenvalues of $\mathbf{G}$ recorded both for $\tau = 0.8$ and for $\tau = 0.35$ correspond to the N uniformly spaced samples of the folded-spectrum over the frequency range $f \in (0, 1/\tau T)$, while the eigenvalues of $\mathbf{H}$ and $\bar{\mathbf{H}}$ have a similar distribution to that of $\mathbf{H}$. To be more specific, the inset in Fig. 2 demonstrates that the eigenvalues of $\mathbf{H}$ are almost the same as that of $\mathbf{G}$, while the eigenvalues of $\bar{\mathbf{H}}$ exhibit only insignificant fluctuations around the corresponding eigenvalues of $\mathbf{H}$, limited to around 10^{-2} to 10^{-4}. More importantly, note that some of the eigenvalues of $\mathbf{G}$, $\bar{\mathbf{H}}$, and $\mathbf{H}$ for $\tau = 0.35$ theoretically approach zero and the number of those eigenvalues is closely related both to the bandwidth of the signaling pulse and to the symbol rate [20]. However, those near-zero eigenvalues would impose performance loss for FDE due to the reduction of the equivalent SNR of the corresponding sub-carriers. For example, at $E_s/N_0 = 10$ dB, we can obtain $\gamma(E_s/N_0) = 2.38$ for $\tau = 0.8$ and $\gamma(E_s/N_0) = 0.28$ for $\tau = 0.35$, which indicates that the significant performance loss due to the near-zero eigenvalues.

Let us now consider channel-coded systems, where the Gaussian priors of the transmitted symbols are transformed to the FD by the FFT. To reduce the complexity of calculations, the TD covariance matrix $\mathbf{V}_x$ is approximated by $\alpha\mathbf{I}_N$ using $\alpha = \frac{\sum_n v_{x_n}}{N}$, with v_{x_n} being the nth diagonal element of $\mathbf{V}_x$ [13]. Consequently, based on the FD *a priori* mean $\mathbf{m}_{x_f}$ and the covariance matrix $\mathbf{V}_{x_f}$, the MMSE estimator is formulated as

$$\hat{\mathbf{x}}_f = \mathbf{W}\left[\mathbf{y}_f - \mathbf{\Lambda}\mathbf{m}_{x_f}\right] + \mathbf{m}_{x_f}. \tag{18}$$

Again, $\mathbf{W}$ is diagonal, facilitating the symbol-by-symbol detection. Finally, we obtain the log likelihood ratios (LLRs) that are fed back to the channel-decoder, expressed as [31]

$$\mathbf{L} = \frac{\mathbf{m}_x \text{tr}[\mathbf{W}\mathbf{\Lambda}]/N + \mathbf{F}^{\mathrm{H}}\hat{\mathbf{x}}_f}{1 + \alpha \cdot \text{tr}[\mathbf{W}\mathbf{\Lambda}]/N}. \tag{19}$$

Remark: The overall complexity of the FDE consists of the detection complexity and the complexity of FFT, which is at the order of $N + N\log N$. On the other hand, the TDE has a complexity order of $N \cdot 2^L$ for BPSK modulation. Generally

[1]The MMSE estimator is equivalent to the ML (MAP) estimator under the Gaussian approximation of data symbols. Directly transforming the *a priori* TD message with discrete values to the FD is possible but it has a complexity even higher than the TDE, which defeats the purposes of employing FDE.

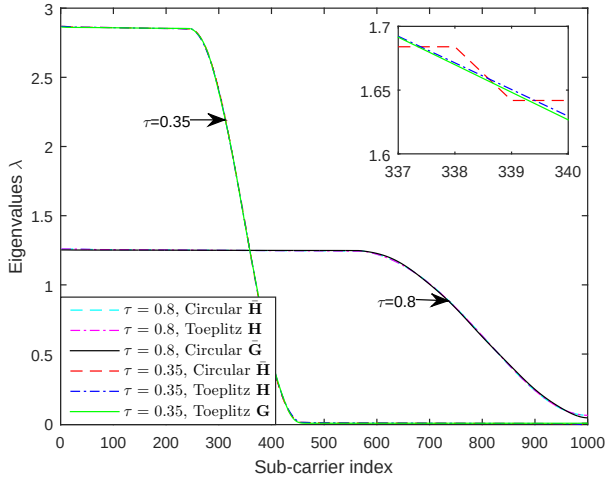

Fig. 2. Eigenvalues λ with different values of τ for the RRC pulse using $\beta = 0.3$.

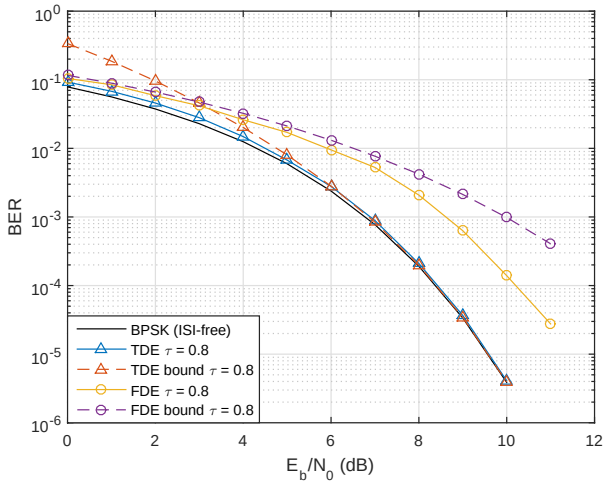

Fig. 3. BER performance comparison of the TDE and the FDE for uncoded FTN signaling systems with $\tau = 0.8$.

speaking, we can conclude that FDE has a significantly lower complexity than that of the TDE for FTN transmissions.

V. Results and Discussions

In this section, we evaluate the error performance of TDE and FDE by means of numerical simulations. In particular, we focus on both coded and uncoded FTN systems with BPSK modulation for $\tau = 0.8$ and $\tau = 0.35$. Without loss of generality, we consider the RRC with a roll-off factor of $\beta = 0.3$ as the signaling pulse and the number of transmitted symbols is set to $N = 1000$. We apply an 8-states BCJR detector for $\tau = 0.8$ and a 256-states BCJR detector for $\tau = 0.35$. On the other hand, the FDE considers $L = 8$ ISI taps for $\tau = 0.8$ and $L = 20$ ISI taps for $\tau = 0.35$.

The BER performance of uncoded FTN systems for $\tau = 0.8$ are given in Fig. 3. It can be observed that the TDE-based detector for $\tau = 0.8$ has a similar BER to that of uncoded BPSK using ISI-free Nyquist signaling, which also shows a close match to the derived performance bound. On the other hand, the FDE-based detector has a performance gap of almost 5 dB with respect to the ISI-free case at BER $\approx 10^{-4}$ for $\tau = 0.8$, which also matches our performance bound. The performance degradation of FDE compared to that of the TDE is mainly due to the Gaussian approximation of transmitted symbols.

Fig. 4 shows the BER performance of uncoded FTN systems for $\tau = 0.35$. As illustrated in the figure, the performance of the TDE-based detector for $\tau = 0.35$ shows an error floor at BER $\approx 10^{-3}$ due to having insufficient trellis states for the BCJR detector. Furthermore, the corresponding performance bound matches well with the actual performance in the high-SNR region, but slightly diverges in the moderate-to-high SNR region since we only consider the expectation of the residual ISI variance. On the other hand, the FDE-based detector fails to detect the FTN signal associated with $\tau = 0.35$. Note that this substantial performance degradation is not only due to the adopted Gaussian approximation, but also owing to the small eigenvalues, as discussed in

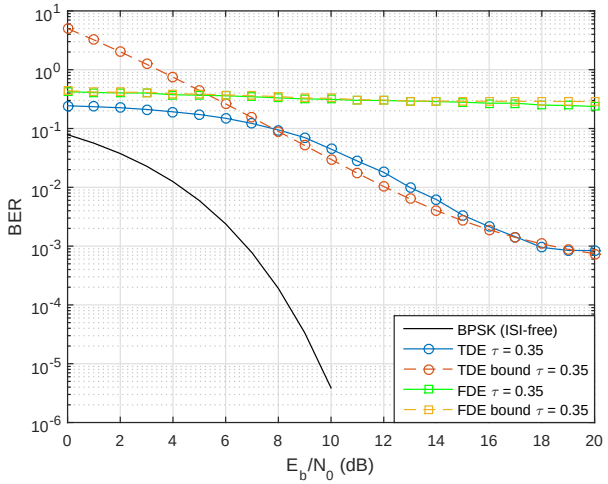

Fig. 4. BER performance comparison of the TDE and the FDE for uncoded FTN signaling systems with $\tau = 0.35$.

Section IV. Overall, the TDE shows substantially superior performance to the FDE for uncoded FTN systems at the cost of a higher computational complexity, which is consistent with our analysis.

The BER performance of convolutionally coded (CC) FTN systems for both $\tau = 0.8$ and $\tau = 0.35$ are given in Fig. 5, where turbo equalization using 20 iterations is performed between the equalizer and decoder. Without loss of generality, we consider a rate-$1/2$ convolutional code, whose generator polynomial is given by $\mathcal{G} = [1 + D^2, 1 + D + D^2]$. The length of the information sequence is 1000 bits and the resultant codeword is of length $N = 2004$, where 4 bits are used to terminate the code trellis. All the parameters used for equalization are the same as those in Fig. 3 and 4. Observe that the TDE is eminently suitable for convolutionally coded FTN systems, since its BER performance approaches that of the ISI-free case for both $\tau = 0.8$ and $\tau = 0.35$ if the SNR is sufficiently high. On the other hand, the BER performance

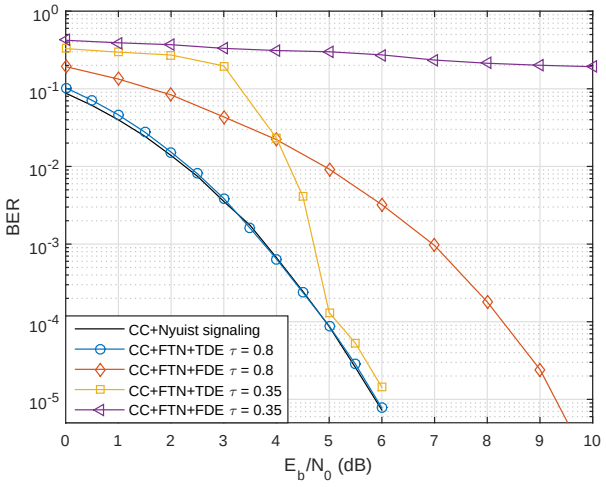

Fig. 5. BER performance comparison of the TDE and the FDE for convolutionally coded FTN signaling systems.

of the FDE falls behind the ISI-free case around 3.2 dB at BER $\approx 10^{-5}$ for $\tau = 0.8$. However, similar to the uncoded system, the FDE fails to perform well for $\tau = 0.35$. This essential performance loss is due to the spectral zeros and the Gaussian approximation.

VI. Conclusion

We have compared the TDE and the FDE for FTN signaling. The FDE imposes a lower complexity based on the circulant structure of the TD channel matrix, even upon taking into account the complexity of the FFT. We found that the Gaussian approximation of data symbols and the near-zero eigenvalues lead to a performance degradation for the FDE, especially for a low packing factor. Our simulation results showed that the FDE fails to reliably detect the data symbols even for coded systems when $\tau = 0.35$, while the TDE is still efficient. For the convolutionally coded FTN transmission with $\tau = 0.8$, the TDE approaches the ISI-free performance bound, while the FDE suffers from a 3.2 dB SNR loss. In summary, the TDE outperforms the FDE for FTN signaling. However, the FDE may be attractive in low-complexity scenarios.

References

[1] J. E. Mazo, "Faster-than-Nyquist signaling," *Bell Syst. Tech. J.*, vol. 54, no. 8, pp. 1451–1462, Aug. 1975.

[2] F. Rusek and J. B. Anderson, "Constrained capacities for faster-than-Nyquist signaling," *IEEE Trans. Inf. Theory*, vol. 55, no. 2, pp. 764–775, Feb. 2009.

[3] S. Li, B. Bai, J. Zhou, Q. He, and Q. Li, "Superposition coded modulation based faster-than-Nyquist signaling," *Wireless Commun. Mobile Comput.*, vol. 2018, 2018.

[4] M. Liu, S. Li, Q. Li, and B. Bai, "Faster-than-Nyquist signaling based adaptive modulation and coding," in *Proc. IEEE Int. Conf. Wireless Commun. Signal Process. (WCSP)*, 2018, pp. 1–5.

[5] W. Yuan, N. Wu, Q. Guo, J. Yuan, D. W. K. Ng, and L. Hanzo, "Iterative joint channel estimation, user activity tracking, and data detection for FTN-NOMA systems supporting random access," *IEEE Trans. Commun.*, vol. 68, no. 5, pp. 2963–2977, May, 2020.

[6] B. Liu, S. Li, Y. Xie, and J. Yuan, "Deep learning assisted sum-product detection algorithm for faster-than-Nyquist signaling," in *Proc. IEEE Inf. Theory Workshop (ITW)*, 2019, pp. 1–5.

[7] S. Li, J. Yuan, and B. Bai, "Code based channel shortening for faster-than-Nyquist signaling," in *Proc. IEEE Int. Conf. Commun.*, Jun. 2020, pp. 1–6.

[8] K. Wang, A. Liu, X. Liang, S. Peng, and Q. Zhang, "A faster-than-nyquist (FTN)-based multicarrier system," *IEEE Trans. Veh. Technol.*, vol. 68, no. 1, pp. 947–951, Jan. 2019.

[9] W. Yuan, N. Wu, A. Zhang, X. Huang, Y. Li, and L. Hanzo, "Iterative receiver design for FTN signaling aided sparse code multiple access," *IEEE Trans. Wireless Commun.*, vol. 23, no. 9, pp. 1270–1274, Feb. 2020.

[10] A. Prlja and J. B. Anderson, "Reduced-complexity receivers for strongly narrowband intersymbol interference introduced by faster-than-Nyquist signaling," *IEEE Trans. Commun.*, vol. 60, no. 9, pp. 2591–2601, Sep. 2012.

[11] S. Li, B. Bai, J. Zhou, P. Chen, and Z. Yu, "Reduced-complexity equalization for faster-than-Nyquist signaling: New methods based on Ungerboeck observation model," *IEEE Trans. Commun.*, vol. 66, no. 3, pp. 1190–1204, Mar. 2017.

[12] C. Zhang, Z. Wang, C. Pan, S. Chen, and L. Hanzo, "Low-complexity iterative frequency domain decision feedback equalization," *IEEE Trans. Veh. Technol.*, vol. 60, no. 3, pp. 1295–1301, Mar. 2011.

[13] S. Sugiura and L. Hanzo, "Frequency-domain-equalization-aided iterative detection of faster-than-Nyquist signaling," *IEEE Trans. Veh. Technol.*, vol. 64, no. 5, pp. 2122–2128, May. 2014.

[14] W. Yuan, N. Wu, H. Wang, and J. Kuang, "Variational inference-based frequency-domain equalization for faster-than-Nyquist signaling in doubly selective channels," *IEEE Signal Process. Lett.*, vol. 19, no. 2, pp. 915–928, Sep. 2016.

[15] Q. Shi, N. Wu, X. Ma, and H. Wang, "Frequency-domain joint channel estimation and decoding for faster-than-Nyquist signaling," *IEEE Trans. Commun.*, vol. 66, no. 2, pp. 781–795, Feb. 2018.

[16] H. Fukumoto and K. Hayashi, "Overlap frequency domain equalization for faster-than-Nyquist signaling," *arXiv preprint arXiv:1509.00562*, 2015.

[17] J. B. Anderson, F. Rusek, and V. Öwall, "Faster-than-Nyquist signaling," *Proc. IEEE*, vol. 101, no. 8, pp. 1817–1830, Aug. 2013.

[18] G. D. Forney, "Maximum-likelihood sequence estimation of digital sequences in the presence of intersymbol interference," *IEEE Trans. Inf. Theory*, vol. 18, no. 3, pp. 363–378, Mar. 1972.

[19] G. Ungerboeck, "Adaptive maximum-likelihood receiver for carrier-modulated data-transmission systems," *IEEE Trans. Commun.*, vol. 22, no. 5, pp. 624–636, May. 1974.

[20] Y. J. D. Kim, "Properties of faster-than-Nyquist channel matrices and folded-spectrum, and their applications," in *Proc. IEEE Wireless Commun. Net. Conf.*, 2016, pp. 1–7.

[21] G. D. Forney and G. Ungerboeck, "Modulation and coding for linear Gaussian channels," *IEEE Trans. Inf. Theory*, vol. 44, no. 6, pp. 2384–2415, Oct. 1998.

[22] B. Vucetic and J. Yuan, *Turbo Codes: Principles and Applications*. Springer Science & Business Media, 2012, vol. 559.

[23] J. Yuan, B. Vucetic, and W. Feng, "Combined Turbo codes and interleaver design," *IEEE Trans. Commun.*, vol. 47, no. 4, pp. 484–487, 1999.

[24] W. Feng, J. Yuan, and B. Vucetic, "A code-matched interleaver design for Turbo codes," *IEEE Trans. Commun.*, vol. 50, no. 6, pp. 926–937, 2002.

[25] S. S. Pietrobon, G. Ungerboeck, L. C. Pérez, and D. Costello, "Rotationally invariant nonlinear trellis codes for two-dimensional modulation," *IEEE Trans. Inf. Theory*, vol. 40, no. 6, pp. 1773–1791, Nov. 1994.

[26] S. Li, J. Yuan, B. Bai, and N. Benvenuto, "Code based channel shortening for faster-than-Nyquist signaling: Reduced-complexity detection and code design," to appear in *IEEE Trans. Commun.*, 2020.

[27] G. Colavolpe and A. Barbieri, "On MAP symbol detection for ISI channels using the ungerboeck observation model," *IEEE Commun. Lett.*, vol. 9, no. 8, pp. 720–722, Aug. 2005.

[28] T. Ishihara and S. Sugiura, "Iterative frequency-domain joint channel estimation and data detection of faster-than-Nyquist signaling," *IEEE Trans. Wireless Commun.*, vol. 16, no. 9, pp. 6221–6231, Sep. 2017.

[29] F. Adachi, H. Tomeba, and K. Takeda, "Frequency-domain equalization for broadband single-carrier multiple access," *IEICE Trans. Commun.*, vol. 92, no. 5, pp. 1441–1456, May. 2009.

[30] Z. Zhu and M. B. Wakin, "On the asymptotic equivalence of circulant and Toeplitz matrices," *IEEE Trans. Inf. Theory*, vol. 63, no. 5, pp. 2975–2992, May 2017.

[31] M. El-Hajjar and L. Hanzo, "EXIT charts for system design and analysis," *IEEE Commun. Sur. & Tut.*, vol. 16, no. 1, pp. 127–153, Jan. 2013.